

Constraints on general neutrino interactions with exotic fermion from neutrino-electron scattering experiments

Zikang Chen,^{1,*} Tong Li,^{2,†} and Jiajun Liao^{1,‡}

¹*School of Physics, Sun Yat-Sen University, Guangzhou 510275, China*

²*School of Physics, Nankai University, Tianjin 300071, China*

Abstract

The couplings between the neutrinos and exotic fermion can be probed in both neutrino scattering experiments and dark matter direct detection experiments. We present a detailed analysis of the general neutrino interactions with an exotic fermion and electrons at neutrino-electron scattering experiments. We obtain the constraints on the coupling coefficients of the scalar, pseudoscalar, vector, axialvector, tensor and electromagnetic dipole interactions from the CHARM-II, TEXONO and Borexino experiments. For the flavor-universal interactions, we find that the Borexino experiment sets the strongest bounds in the low mass region for the electromagnetic dipole interactions, and the CHARM-II experiment dominates the bounds for other scenarios. If the interactions are flavor dependent, the bounds from the CHARM-II or TEXONO experiment can be avoided, and there are correlations between the flavored coupling coefficients for the Borexino experiment. We also discuss the detection of sub-MeV DM absorbed by bound electron targets and illustrate that the vector coefficients preferred by XENON1T data is allowed by the neutrino experiments.

* chenzk7@mail2.sysu.edu.cn

† litong@nankai.edu.cn

‡ liaojiajun@mail.sysu.edu.cn

I. INTRODUCTION

The phenomenon of neutrino oscillations has been well confirmed by various neutrino experiments in the last two decades [1]. Since the explanation of neutrino oscillations requires nonvanishing neutrino masses, which cannot be accounted for by the Standard Model (SM), the observation of neutrino oscillations provides a strong motivation to search for new physics beyond the SM that are associated with neutrinos. Moreover, the existence of dark matter (DM) through abundant cosmological and astrophysical observations is one of the most plausible evidences of new physics beyond the SM. The DM direct detection experiments have pushed the limit on the cross section of DM scattering off nucleus close to the neutrino floor for weak scale DM. The couplings between the neutrinos and sub-GeV DM through the scattering off nucleus have been studied in Ref. [2–9]. There are also plenty of novel models and signatures proposed to search for sub-GeV DM through the scattering off electrons [10–15].

Recently, the XENON collaboration reported an excess of electronic recoil events with the energy around 2-3 keV [16] and the event distribution has a broad spectrum for the excess. They collected low energy electron recoil data from the XENON1T experiment with an exposure of 0.65 tonne-years and analyzed various backgrounds for the excess events. Although a small tritium background fits the excess data well, the solar axion explanation or the solar neutrinos with magnetic moment can also provide a plausible source for the peak-like excess. However, both of the two scenarios have tension with stellar cooling constraints [14, 17–21]. Some studies instead proposed to explain the XENON1T excess through the electron recoil by solar neutrinos with the sterile neutrino DM in the final states of inelastic scattering [10–12]. On the other hand, the inverse process in which the incoming fermionic DM is absorbed by bound electron targets and emits a neutrino is sensitive to the DM with mass below MeV [13]. The two kinds of signals are governed by the same interactions between SM neutrino and the exotic fermion. The relevant interactions are inevitably constrained by the precision measurements in neutrino experiments [14, 15]. In this work we study the constraints on general neutrino interactions with sub-GeV exotic fermion from neutrino-electron scattering experiments.

The large volume detectors enable precise measurements of neutrino properties. The large neutrino detectors like Borexino can be used to place constraints on general neutrino interactions. The Borexino experiment, located at the Laboratori Nazionali del Gran Sasso, was built with a primary goal of measuring solar neutrinos from the pp chain [22]. We employ the Borexino measurements of low energy solar neutrinos to set limits on the neutrino-electron scattering with an outgoing fermion χ

$$\nu e \rightarrow \chi e, \quad (1)$$

where χ could be sterile neutrino or other possible exotic fermions. The results apply for the exotic fermion χ being either DM candidate or not. We restrict the general neutrino interactions categorized by dimension-5 dipole operators and dimension-6 four-fermion operators. They respect Lorentz invariance and the gauge symmetries $SU(3)_c \times U(1)_{\text{em}}$. The scattering cross section from

the magnetic and electric dipole operators is inversely proportional to the recoil energy and thus the experiments with low energy threshold are sensitive to them. For the four-fermion interactions, all Lorentz-invariant operators (scalar, vector, pseudoscalar, axialvector and tensor) will be explored in the neutrino-electron scattering. As the produced solar electron neutrinos oscillate into muon and tau neutrinos, we can also place limits on the general interactions of all neutrino flavors. In addition, accelerator neutrinos with the energy being several tens of GeV can be used to exploit large χ mass region. We thus take into account the constraints from the CHARM-II experiment [23, 24] as well as reactor neutrino using TEXONO [25] data.

This paper is organized as follows. In Sec. II, we discuss the effective Lagrangian of an exotic fermion interacting with neutrino and electron. Then we display the amplitudes and differential cross sections of neutrino-electron scattering with the outgoing exotic fermion. In Sec. III, we consider three neutrino-electron scattering experiments: CHARM-II, TEXONO and Borexino, and show the constraints on the general neutrino interactions. Finally, we discuss the detection of sub-MeV DM absorbed by bound electron targets and summarize our conclusions in Sec. V.

II. THE GENERAL NEUTRINO INTERACTIONS WITH EXOTIC FERMION AND NEUTRINO-ELECTRON SCATTERING

We consider a Dirac fermion χ and its general interactions with neutrino and electron. The effective Lagrangian including both dim-5 dipole operators and dim-6 four-fermion operators reads as

$$\mathcal{L} \supset \frac{G_F}{\sqrt{2}} \left[\sum_a \bar{\chi} \Gamma^a \nu_\alpha \bar{e} \Gamma^a (\epsilon_\alpha^a + \tilde{\epsilon}_\alpha^a \gamma^5) e + \frac{v_H}{\sqrt{2}} \bar{\chi} \sigma^{\mu\nu} (\epsilon_\alpha^M + \epsilon_\alpha^E \gamma_5) \nu_\alpha F_{\mu\nu} \right] + h.c. , \quad (2)$$

where $\alpha \equiv \{e, \mu, \tau\}$, $v_H \simeq 246$ GeV is the vacuum expectation value of the SM Higgs, $F_{\mu\nu}$ is the electromagnetic field strength tensor and $\Gamma^a \equiv \{I, i\gamma^5, \gamma^\mu, \gamma^\mu \gamma^5, \sigma^{\mu\nu} \equiv \frac{i}{2}[\gamma^\mu, \gamma^\nu]\}$ correspond to the scalar (S), pseudoscalar (P), vector (V), axialvector (A) and tensor (T) operator, respectively. The four-fermion operators are analogous to those in Ref. [26]. Here the dimensionless parameters ϵ_α^M , ϵ_α^E , ϵ_α^a and $\tilde{\epsilon}_\alpha^a$ are in general complex. The presence of new interactions of Eq. (2) will give rise to the tree-level neutrino-electron scattering, as shown in Fig. 1.

In the SM, the neutrino-electron scattering is governed by both the weak neutral current (NC) and charged current (CC). The effective Lagrangian for the SM NC is given by

$$\mathcal{L}_{\text{NC}} = \frac{G_F}{\sqrt{2}} \bar{\nu} \gamma^\mu (1 - \gamma_5) \nu \bar{e} \gamma_\mu (g_V - g_A \gamma_5) e , \quad (3)$$

where $g_V = -\frac{1}{2} + 2 \sin^2 \theta_W$ and $g_A = -\frac{1}{2}$. The CC Lagrangian can be transmitted as

$$\mathcal{L}_{\text{CC}} = \frac{G_F}{\sqrt{2}} \bar{\nu} \gamma^\mu (1 - \gamma_5) \nu \bar{e} \gamma_\mu (1 - \gamma_5) e . \quad (4)$$



FIG. 1. The tree-level Feynman diagrams for the $\nu_\alpha + e^- \rightarrow \chi + e^-$ process, where the circular bulb (square) represents the effective dim-5 dipole (dim-6 four-fermion) interaction.

The CC current only contributes to the scattering of ν_e . The differential cross section of neutrino-electron scattering in the SM is [26]

$$\frac{d\sigma_{\alpha\beta}^{\text{SM}}}{dE_R} = \frac{G_F^2 m_e}{2\pi} \left[\left(g_{\alpha\beta}^L \right)^2 + \left(g_{\alpha\beta}^R \right)^2 \left(1 - \frac{E_R}{E_\nu} \right)^2 - g_{\alpha\beta}^L g_{\alpha\beta}^R \frac{m_e E_R}{E_\nu^2} \right], \quad (5)$$

where α (β) denotes the flavor of the neutrino in the initial (final) states, E_ν is the neutrino energy, E_R is the electron recoil energy and

$$\left(g_{\alpha\beta}^L, g_{\alpha\beta}^R \right) = \begin{cases} (2 \sin^2 \theta_W + 1, 2 \sin^2 \theta_W), & \alpha = \beta = e; \\ (2 \sin^2 \theta_W - 1, 2 \sin^2 \theta_W), & \alpha = \beta = \mu, \tau; \\ 0, & \alpha \neq \beta. \end{cases} \quad (6)$$

We then calculate the differential cross section of $\nu_\alpha + e \rightarrow \chi + e$ by following the procedure given in the appendix. Here we show the differential cross sections for different operators:

$$\frac{d\sigma_{\nu\alpha}^S}{dE_R} = \frac{G_F^2 m_e}{8\pi} \left[|\epsilon_\alpha^S|^2 \left(1 + \frac{E_R}{2m_e} \right) + |\tilde{\epsilon}_\alpha^S|^2 \frac{E_R}{2m_e} \right] \left(\frac{m_e E_R}{E_\nu^2} + \frac{m_\chi^2}{2E_\nu^2} \right), \quad (7)$$

$$\frac{d\sigma_{\nu\alpha}^P}{dE_R} = \frac{G_F^2 m_e}{8\pi} \left[|\epsilon_\alpha^P|^2 \frac{E_R}{2m_e} + |\tilde{\epsilon}_\alpha^P|^2 \left(1 + \frac{E_R}{2m_e} \right) \right] \left(\frac{m_e E_R}{E_\nu^2} + \frac{m_\chi^2}{2E_\nu^2} \right), \quad (8)$$

$$\begin{aligned} \frac{d\sigma_{\nu\alpha}^V}{dE_R} = & \frac{G_F^2 m_e}{4\pi} \left[(|\epsilon_\alpha^V|^2 + |\tilde{\epsilon}_\alpha^V|^2) \left(1 - \frac{E_R}{E_\nu} + \frac{E_R^2}{2E_\nu^2} - \frac{m_\chi^2}{2E_\nu m_e} + \frac{m_\chi^2 E_R}{4E_\nu^2 m_e} \right) \right. \\ & \left. - (|\epsilon_\alpha^V|^2 - |\tilde{\epsilon}_\alpha^V|^2) \left(\frac{E_R m_e}{2E_\nu^2} + \frac{m_\chi^2}{4E_\nu^2} \right) - 2\text{Re}[\epsilon_\alpha^V (\tilde{\epsilon}_\alpha^V)^*] \frac{E_R}{E_\nu} \left(1 - \frac{E_R}{2E_\nu} - \frac{m_\chi^2}{4E_\nu m_e} \right) \right], \quad (9) \end{aligned}$$

$$\begin{aligned} \frac{d\sigma_{\nu\alpha}^A}{dE_R} = & \frac{G_F^2 m_e}{4\pi} \left[(|\epsilon_\alpha^A|^2 + |\tilde{\epsilon}_\alpha^A|^2) \left(1 - \frac{E_R}{E_\nu} + \frac{E_R^2}{2E_\nu^2} - \frac{m_\chi^2}{2E_\nu m_e} + \frac{m_\chi^2 E_R}{4E_\nu^2 m_e} \right) \right. \\ & \left. + (|\epsilon_\alpha^A|^2 - |\tilde{\epsilon}_\alpha^A|^2) \left(\frac{E_R m_e}{2E_\nu^2} + \frac{m_\chi^2}{4E_\nu^2} \right) - 2\text{Re}[\epsilon_\alpha^A (\tilde{\epsilon}_\alpha^A)^*] \frac{E_R}{E_\nu} \left(1 - \frac{E_R}{2E_\nu} - \frac{m_\chi^2}{4E_\nu m_e} \right) \right], \quad (10) \end{aligned}$$

$$\frac{d\sigma_{\nu\alpha}^T}{dE_R} = \frac{2G_F^2 m_e |\epsilon_\alpha^T - \tilde{\epsilon}_\alpha^T|^2}{\pi} \left[1 - \frac{E_R}{E_\nu} + \frac{E_R^2}{4E_\nu^2} - \frac{E_R m_e}{4E_\nu^2} - \frac{m_\chi^2}{4E_\nu^2} \left(\frac{1}{2} + \frac{2E_\nu}{m_e} - \frac{E_R}{2m_e} \right) \right], \quad (11)$$

$$\frac{d\sigma_{\nu\alpha}^{\text{EM}}}{dE_R} = \frac{2\sqrt{2}\alpha_{\text{EM}} G_F |\epsilon_\alpha^E - \epsilon_\alpha^M|^2}{m_e} \left[\frac{m_e}{E_R} - \frac{m_e}{E_\nu} - \frac{m_\chi^2}{E_\nu E_R} \left(\frac{1}{2} - \frac{E_R}{4E_\nu} + \frac{m_e}{E_\nu} \right) - \frac{m_\chi^4}{8E_\nu^2 E_R^2} \left(1 - \frac{E_R}{m_e} \right) \right] \quad (12)$$

where $\alpha_{\text{EM}} \simeq 1/137$ is the electromagnetic fine structure constant. Here we assume each of the scalar, pseudoscalar, vector, axialvector, tensor and electromagnetic dipole operators dominates at a time. The differential cross sections of $\bar{\nu}_\alpha + e \rightarrow \bar{\chi} + e$ are the same as those of $\nu_\alpha + e \rightarrow \chi + e$ except for the cross term of the axialvector operator in Eq. (10) changed sign. From the above equations, we realize that the the bounds on $\{\tilde{\epsilon}_\alpha^S, \tilde{\epsilon}_\alpha^P, \tilde{\epsilon}_\alpha^V, \tilde{\epsilon}_\alpha^A, \tilde{\epsilon}_\alpha^T, \epsilon_\alpha^E\}$ will be the same as $\{\epsilon_\alpha^P, \epsilon_\alpha^S, \epsilon_\alpha^A, \epsilon_\alpha^V, \epsilon_\alpha^T, \epsilon_\alpha^M\}$ if we consider only one ϵ parameter at a time.

III. NEUTRINO-ELECTRON SCATTERING EXPERIMENTS

In our analysis, we consider three neutrino-electron scattering experiments: CHARM-II, TEXONO and Borexino. Other neutrino-electron scattering experiments such as GEMMA [27] and LSND [28] can be also used to constrain the parameter space. However, we find their sensitivities are weaker compared to those from CHARM-II, TEXONO and Borexino experiments. Here we present the detailed analysis of the CHARM-II, TEXONO and Borexino experiments below.

A. CHARM-II

The CHARM-II experiments measured the high energy ν_μ and $\bar{\nu}_\mu$ beam from the Super Proton Synchrotron (SPS) at CERN [23, 24]. The mean neutrino energies of the ν_μ and $\bar{\nu}_\mu$ beam are 23.7 GeV and 19.1 GeV, respectively. The unfolded differential cross sections from the measurement have been given in Ref. [23], and the data points are shown in Fig. 2. Our SM predictions are consistent with those given in the Ref. [23]. Therefore, we consider the following χ^2 function in our analysis for new physics:

$$\chi_{\text{CHARM-II}}^2 = \sum_i \frac{(d\sigma/dE_R)_i - s_i^0)^2}{\sigma_i^2} + (\nu_\mu \rightarrow \bar{\nu}_\mu), \quad (13)$$

where s_i^0 and σ_i are the measured differential cross section and its corresponding uncertainties taken from Ref. [23].

B. TEXONO

The cross section of $\bar{\nu}_e$ scattering on electrons has been measured by the TEXONO experiment utilizing electron antineutrinos produced by the Kuo-Sheng Nuclear Power Reactor with a CsI(Tl) scintillating crystal detector [25]. The detector is placed at a distance of 28 m from the 2.9 GW reactor core. The range of recoil energy used in the analysis is from 3 MeV and 8 MeV, respectively. The measured event rates and uncertainties have been given in Ref. [25], which are shown in Fig. 3. As seen from the red and blue dashed curves in Fig. 3, our SM predictions agree quite well with those given in the Ref. [25]. Therefore, we consider the following χ^2 function in our

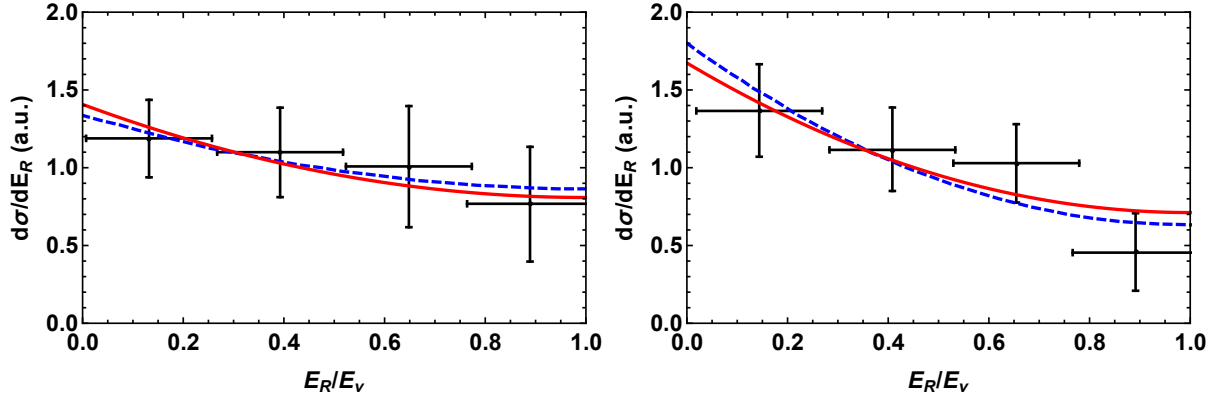


FIG. 2. The differential cross sections of the ν_μ (left) and $\bar{\nu}_\mu$ (right) scattering on electrons at CHARM-II. The black data points and the blue dashed SM prediction curve are taken from Ref. [23]. The red curve corresponds to our best-fit prediction in the SM.

analysis for new physics:

$$\chi_{\text{TEXONO}}^2 = \sum_i \frac{(R_i^0 - R_i(1 + \alpha))^2}{\sigma_{R,i}^2} + \left(\frac{\alpha}{\sigma_\alpha} \right)^2, \quad (14)$$

where R_i (R_i^0) and $\sigma_{R,i}$ are the predicted (measured) event rates and corresponding uncertainties in the i th recoil energy bin. Here σ_α is the normalization uncertainty, and we take it to be 5% for conservation. Both the measured event rates and uncertainties are taken from Ref. [25]. The predicted event rate in the i th recoil energy bin is calculated by

$$R_i = N_e \int dE_\nu \phi_{\bar{\nu}_e}(E_\nu) \int_i dE_R \frac{d\sigma_{\bar{\nu}_e}}{dE_R}, \quad (15)$$

where $N_e = 2.5 \times 10^{26}$ is the number of target electrons in the CsI detector per kilogram, $\phi_{\bar{\nu}_e}(E_\nu)$ is the reactor antineutrino flux taken from Ref. [25] and the total flux is normalized to $6.4 \times 10^{12} \text{ cm}^{-1} \text{ s}^{-1}$.

C. Borexino

The Borexino experiment measured solar neutrinos at the Laboratori Nazionali del Gran Sasso. Only ν_e are produced in the core of the Sun. However, after adiabatic propagation in the sun, the solar neutrinos arrive at the Earth contain all three flavors: ν_e , ν_μ and ν_τ . The survival probability of solar neutrinos is given by [29]

$$P_{ee} \approx s_{13}^4 + c_{13}^4 (c_{12}^2 \cos^2 \theta_{12}^m + s_{12}^2 \sin^2 \theta_{12}^m), \quad (16)$$

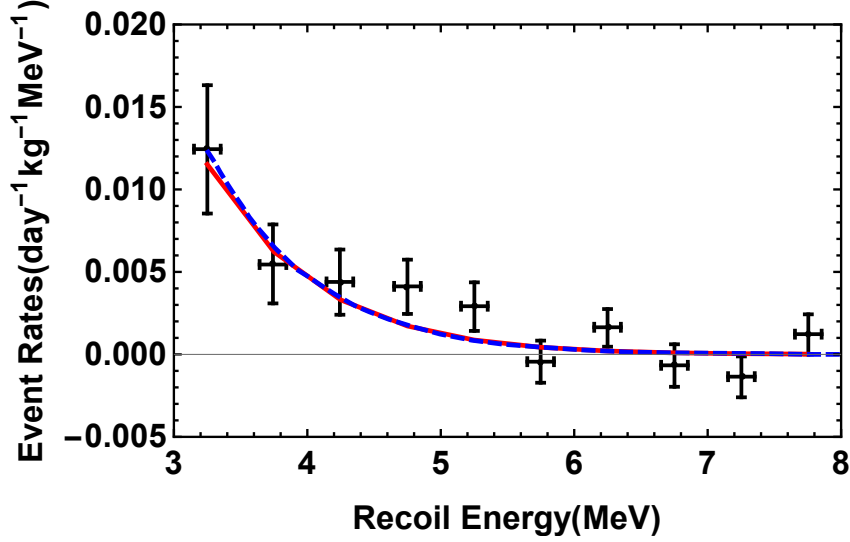


FIG. 3. The event rates of $\bar{\nu}_e - e^-$ scattering in the TEXONO experiment. The black data points and the blue dashed SM prediction curve are taken from Ref. [25]. The red curve corresponds to our best-fit prediction in the SM.

where s_{12} (c_{12}) denotes $\sin \theta_{12}$ ($\cos \theta_{12}$), θ_{12} is the vacuum mixing angles in the PMNS matrix. Here θ_{12}^m is the effective mixing angle at the production point in the Sun, which is given by

$$\theta_{12}^m = \frac{1}{2} \arctan \frac{\sin 2\theta_{12}}{\cos 2\theta_{12} - \hat{A}c_{13}^2}, \quad (17)$$

with $\hat{A} \equiv 2\sqrt{2}G_F N_e^S E_\nu / \delta m_{21}^2$ and N_e^S being the number density of electron at the production point in the Sun. Here we ignore the small corrections due to the day-night asymmetry in the Borexino measurement [30]. We consider the pp , ${}^7\text{Be}$ and pep spectra measured in the Borexino phase-I [31–33] and phase-II [22, 34], and the ${}^8\text{B}$ data collected between January 2008 and December 2016 [35]. The expected event rate at Borexino is given by

$$R_{\text{pre}}^i = N_e \int dE_\nu \Phi^i(E_\nu) [P_{ee}^i \sigma_e(E_\nu) + (1 - P_{ee}^i) \sigma_\mu(E_\nu)], \quad (18)$$

where $N_e = 3.307 \times 10^{31}/100$ ton is the density of target electrons in the Borexino detector [22], and i indicates solar neutrino sources pp , ${}^7\text{Be}$, pep and ${}^8\text{B}$. $\Phi^i(E_\nu)$ is the corresponding solar neutrino flux taken from the standard solar model (B16-GS98-HZ) [36]. P_{ee}^i is the survival probability given in Eq. (16). The cross section in Eq. (18) is calculated by

$$\sigma_\alpha = \int dE_R \frac{d\sigma_\alpha}{dE_R} \eta(E_R), \quad (19)$$

where $\alpha = e, \mu$, $\frac{d\sigma_\alpha}{dE_R}$ is the differential cross section, and $\eta(E_R)$ is the detection efficiency. We extract the detection efficiency for ${}^8\text{B}$ from Fig. 2 in Ref. [35] and take it as unity for other neutrino

| Source | Measurement (cpd/100 t) | SM prediction (cpd/100 t) | Percentage error |
|-----------------|---|---------------------------|------------------|
| pp | $134 \pm 10^{+6}_{-10}$ | 136.0 ± 1.6 | 1.2% |
| ${}^7\text{Be}$ | $46 \pm 1.5^{+1.5}_{-1.6}$ (phase I), $48.3 \pm 1.1^{+0.4}_{-0.7}$ (phase II) | 47.6 ± 2.9 | 6.1% |
| pep | $3.1 \pm 0.6 \pm 0.3$ (phase I), $2.43 \pm 0.36^{+0.15}_{-0.22}$ (phase II) | 2.76 ± 0.04 | 1.3% |
| ${}^8\text{B}$ | $0.223^{+0.015}_{-0.016} \pm 0.006$ | 0.209 ± 0.025 | 12.0% |

TABLE I. The measured event rates at Borexino and our predicted event rates in the SM. The theoretical percentage uncertainties are given in the last column.

sources. The measured event rates and our predicted event rates in the SM are given in Table I. We see that our SM predictions agree with the measured event rates. For new physics analysis, we employ the following χ^2 function [26]:

$$\chi^2_{\text{Borexino}} = \sum_i \frac{[R_{\text{exp}}^i - R_{\text{pre}}^i(1 + \alpha_i)]^2}{(\sigma_{\text{stat}}^i)^2} + \left(\frac{\alpha^i}{\sigma_{\text{th}}^i}\right)^2, \quad (20)$$

where R_{exp}^i (σ_{exp}^i) are the central values (statistical uncertainties) of the i th measurement given in Table I, R_{pre}^i is the predicted event rates calculated in Eq. (18), and σ_{th}^i is the theoretical uncertainties given in the last column in Table I.

IV. CONSTRAINTS FROM THE EXPERIMENTAL DATA

In this section, we present our results of the constraints on the coupling coefficients of the general neutrino interactions with χ and electrons using the neutrino-electron scattering data from the CHARM-II, TEXONO and Borexino experiments.

A. Flavor-universal bounds

We firstly consider the flavor-universal couplings, i.e. by setting $\epsilon_\alpha^i \equiv \epsilon^i$ in Eq. (2), where i indicates the scalar (S), pseudoscalar (P), vector(V), axialvector (A), tensor (T) and electromagnetic (E or M) dipole operators. Here we also assume only one ϵ^i ($\tilde{\epsilon}^i$) exists at a time. As mentioned before, the bounds on $\{\tilde{\epsilon}_\alpha^S, \tilde{\epsilon}_\alpha^P, \tilde{\epsilon}_\alpha^V, \tilde{\epsilon}_\alpha^A, \tilde{\epsilon}_\alpha^T, \tilde{\epsilon}_\alpha^E\}$ will be the same as $\{\epsilon_\alpha^P, \epsilon_\alpha^S, \epsilon_\alpha^A, \epsilon_\alpha^V, \epsilon_\alpha^T, \epsilon_\alpha^M\}$ in this case. The 90% CL upper bounds on the magnitude of the coefficients ϵ^i ($\tilde{\epsilon}^i$) as a function of m_χ are shown in Fig. 4. From Fig. 4, we see that the CHARM-II experiment yields the strongest bounds for the scalar, pseudoscalar, vector, axialvector and tensor interactions. For the electromagnetic dipole interaction, the Borexino experiment has the best sensitivity for m_χ below 1 MeV. There is an upper limit on m_χ for the CHARM-II bounds due to the kinematic constraint. This can be explained by Eq. (A6), from which we get $m_\chi \leq \sqrt{(2E_\nu + m_e)m_e} - m_e \simeq 155$ MeV for $E_\nu = 23.7$ GeV. Also, the upper limits on m_χ from the TEXONO and Borexino experiments are

much smaller than the CHARM-II experiment due to low neutrino energies used in these two experiments. In addition, we see that the bounds become flat at small m_χ , which can be understood from Eqs. (7), (8), (9), (10), (11) and (12) since the differential cross sections are insensitive to m_χ as $m_\chi \ll E_\nu$. From Fig. 4, we find that for $m_\chi \lesssim 50$ MeV, the strongest bounds on the magnitude of $\epsilon^{S,P}$ ($\tilde{\epsilon}^{S,P}$), $\epsilon^{V,A}$ ($\tilde{\epsilon}^{V,A}$) and ϵ^T ($\tilde{\epsilon}^T$) can reach 1.0, 0.5 and 0.2, respectively. The strongest bounds on the magnitude of $\epsilon^{M,E}$ can reach 1.3×10^{-6} for $m_\chi \lesssim 0.1$ MeV.

B. Flavor-dependent bounds

Since only ν_μ ($\bar{\nu}_\mu$) are measured at the CHARM-II experiment and only $\bar{\nu}_e$ are measured at the TEXONO experiment, the bounds from these two experiments can be avoided if the coupling coefficients are flavor non-universal. To illustrate the flavor dependence of these bounds, we show the 90% CL allowed regions in the $(\epsilon_e, \epsilon_\mu)$ plane for the scalar and vector interactions in Fig. 5. Here we fixed $m_\chi = 1$ MeV, and assume the coupling coefficients are real for simplicity. We also assume $\epsilon_\tau = \epsilon_\mu$ for the Borexino experiments. As seen from Fig. 5, the CHARM-II experiment is not sensitive to ϵ_e , and the TEXONO experiment has no sensitivity to ϵ_μ . The solar neutrino experiment at Borexino can impose constraints on both ϵ_e and ϵ_μ due to the flavor transition in the Sun. We also show the allowed regions of the combined data from these three experiments as the gray shaded regions in Fig. 5. From Fig. 5, one can see that the sensitivity of the combined data mainly comes from the CHARM-II and TEXONO experiment.

V. DISCUSSION AND CONCLUSION

As stated in the Introduction, the exotic fermion χ could or could not be a DM particle. Here we briefly discuss the detection of DM hypothesis and the XENON1T excess. If we reverse the above process and interpret the exotic fermion χ as DM particle, the incoming DM χ can be absorbed by bound electron targets and emit a neutrino

$$\chi e \rightarrow \nu e . \quad (21)$$

For the DM elastic scattering off the electron, to explain the XENON1T excess, the key point is how to produce abundant DM particles with high velocity $v_{\text{DM}} \gtrsim 0.1$ [37]. In contrast, Ref. [13] proposed the above DM absorption scenario in which a DM particle deposits its mass energy rather than kinetic energy and it is sensitive to sub-MeV fermionic DM. For the DM absorption with free electrons $\chi e \rightarrow \nu e$, analogous to the case with nucleus absorbing the DM [4, 5], the total event rate is naively given by

$$R = \frac{\rho_\chi}{m_\chi} \sigma_e N_T \Theta(E_R^0 - E_{\text{th}}) , \quad (22)$$

where N_T is the number of target nuclei per detector mass, the local DM density is $\rho_\chi \simeq 0.4 \text{ GeV}/\text{cm}^3$, Θ is the Heaviside theta function, E_{th} is the experimental threshold, $E_R^0 = m_\chi^2/2m_e$

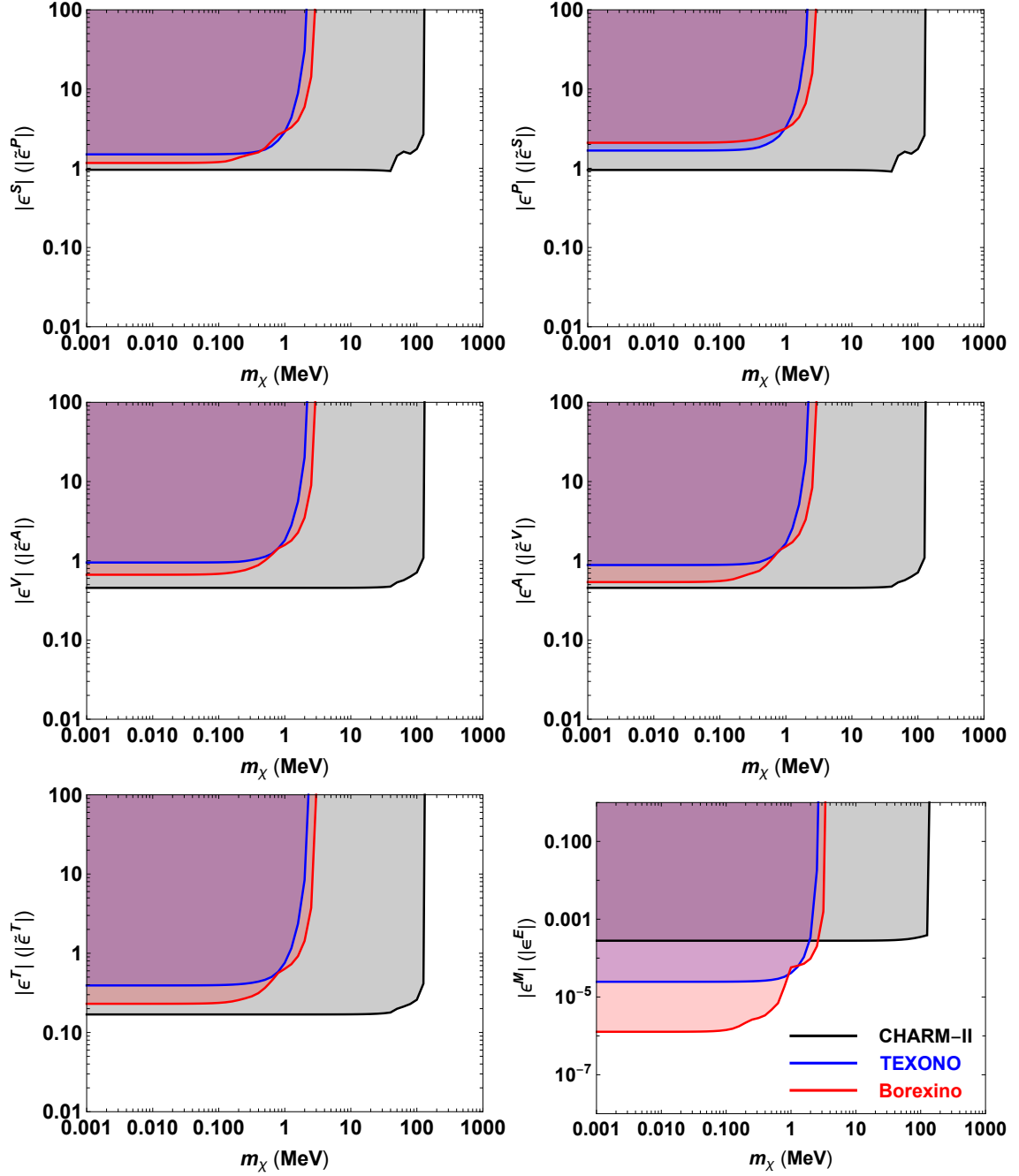


FIG. 4. The 90% CL upper bounds on the magnitude of coupling coefficients as a function of m_χ for the scalar, pseudoscalar, vector, axialvector, tensor and electromagnetic dipole interactions. We assume that the couplings are flavor universal and only one ϵ^i ($\tilde{\epsilon}^i$) exists at a time. The gray, blue and red shaded regions are excluded by the CHARM-II, TEXONO and Borexino experiment, respectively. The bounds on $|\tilde{\epsilon}_\alpha^S|$, $|\tilde{\epsilon}_\alpha^P|$, $|\tilde{\epsilon}_\alpha^V|$, $|\tilde{\epsilon}_\alpha^A|$, $|\tilde{\epsilon}_\alpha^T|$, and $|\epsilon_\alpha^E|$ are the same as $|\epsilon_\alpha^P|$, $|\epsilon_\alpha^S|$, $|\epsilon_\alpha^A|$, $|\epsilon_\alpha^V|$, $|\epsilon_\alpha^T|$, and $|\epsilon_\alpha^M|$, respectively.

for a free electron absorbing the DM, and σ_e is the absorption cross section per electron. For the XENON1T experiment, we have $N_T \simeq 4 \times 10^{27}/\text{tonne}$ and $E_R^0 \simeq 2 \text{ keV}$ giving $m_\chi \simeq 45 \text{ keV}$.

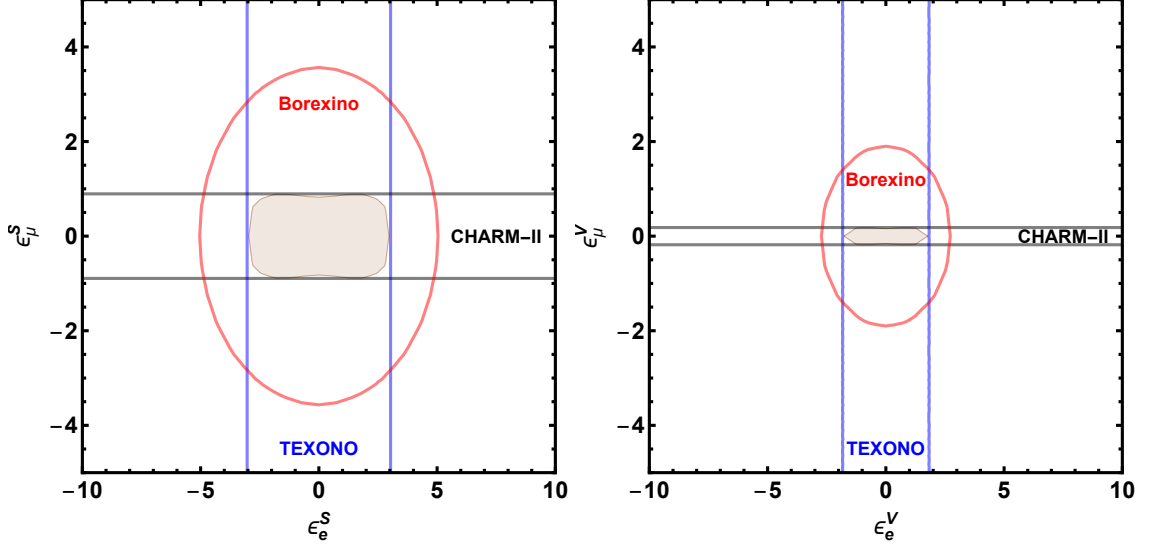


FIG. 5. The 90% CL allowed regions in the $(\epsilon_e, \epsilon_\mu)$ plane for the scalar (left panel) and vector (right panel) interactions. Here we assume $m_\chi = 1$ MeV and the coupling coefficients are real with $\epsilon_\tau = \epsilon_\mu$. The region enclosed by the black, blue and red curves correspond to the CHARM-II, TEXONO and Borexino experiments, respectively. The gray shaded regions correspond to the allowed regions of the combined data from these three experiments.

With the total exposure being 0.65 tonne-years, XENON1T observed 285 events and the expected event number is 232 ± 15 . This gives the total scattering cross section $\sigma_e \simeq 2 \times 10^{-48} \text{ cm}^2$. In fact, the absorbing electron in a shell with a binding energy would be ionized with recoil energy [38, 39]. In Eq. (22) there should also appear the ionization form factor of an electron in a certain shell and the total differential ionization rate is obtained by summing over all possible shells of the absorbing target electrons. The recoil energy of a free electron absorbing the DM E_R^0 is then shifted. The best fit to the XENON1T data was found to be $(m_\chi = 56.5 \text{ keV}, \sigma_e = 1 \times 10^{-49} \text{ cm}^2)$ [13]. We take the vector interaction for illustration. The total scattering cross section σ_e for vector operators is

$$\sigma_e^V = \frac{G_F^2 m_\chi^2 (m_\chi + 2m_e)^2}{32\pi(m_e + m_\chi)^4} \left[|\epsilon^V|^2 (2m_e^2 + 4m_e m_\chi + 3m_\chi^2) + |\tilde{\epsilon}^V|^2 (6m_e^2 + 8m_e m_\chi + 3m_\chi^2) \right] \quad (23)$$

By transforming the above best fit to the parameterization in our context, one essentially obtains $|\epsilon^V|, |\tilde{\epsilon}^V| \simeq 0.1$ which is allowed by the neutrino scattering experiments.

The decaying DM scenario usually faces the requirement of stability. The corresponding lifetime of χ should be longer than the age of the Universe, i.e. $t_{\text{Universe}} = 4.4 \times 10^{17} \text{ sec}$ [40]. Requiring the DM being stable at the Universe time scale would set a very stringent bound on the coupling and/or the DM mass. For the vector interaction in our effective framework, the leading decay process is $\chi \rightarrow \nu\gamma$ with one photon radiated from the closed electron loop. The constraint would be quite stringent if only electron is involved in the calculation of the above decay width. In

a realistic UV model in Ref. [13] with χ only coupled to right-handed neutrino, the decay $\chi \rightarrow \nu\gamma$ is suppressed by the insertion of neutrino mass. The decay of χ into $\nu\gamma\gamma$ is forbidden and the leading decay becomes $\chi \rightarrow \nu\gamma\gamma\gamma$ which leads to a quite weak constraint. We refer the detailed discussion of the sub-MeV DM absorption by electrons to Ref. [13] and future studies.

In this work we study the constraints on general neutrino interactions with sub-GeV exotic fermion χ from neutrino-electron scattering experiments. The general neutrino interactions are composed of dimension-5 dipole operators and dimension-6 four-fermion operators. We employ the measurements of CHARM-II, TEXONO and Borexino experiments to set limits on the neutrino-electron scattering with an outgoing fermion χ . We find that the bounds are dominated by the CHARM-II experiment in most of the parameter space for the flavor-universal interactions and m_χ below 155 MeV, while the Borexino experiment sets the strongest bounds in the low mass region for the electromagnetic dipole interactions. The limits are found to be $|\epsilon^{S,P}|(|\tilde{\epsilon}^{S,P}|) < 1$, $|\epsilon^{V,A}|(|\tilde{\epsilon}^{V,A}|) < 0.5$, $|\epsilon^T|(|\tilde{\epsilon}^T|) < 0.2$ for $m_\chi \lesssim 50$ MeV and $|\epsilon^{M,E}| < 1.3 \times 10^{-6}$ for $m_\chi \lesssim 0.1$ MeV. If the coupling coefficients are flavor non-universal, the bounds on ϵ_e (ϵ_μ) can be avoided for the CHARM-II (TEXONO) experiment, and there are correlations between the bounds on the coupling coefficients from the Borexino experiment. Finally, as an example, we discuss the detection of sub-MeV DM absorbed by bound electron targets. By transforming the best fit to the XENON1T data in our parameterization, we obtain the preferred coefficients for vector interactions as $|\epsilon^V|, |\tilde{\epsilon}^V| \simeq 0.1$ which is allowed by the neutrino experiments.

ACKNOWLEDGMENTS

TL is supported by the National Natural Science Foundation of China (Grant No. 11975129, 12035008) and “the Fundamental Research Funds for the Central Universities”, Nankai University (Grant No. 63196013). JL is supported by the National Natural Science Foundation of China (Grant No. 11905299), Guangdong Basic and Applied Basic Research Foundation (Grant No. 2020A1515011479), the Fundamental Research Funds for the Central Universities, and the Sun Yat-Sen University Science Foundation.

Appendix A: Calculation of the differential cross section

The amplitude for $\nu(p_1)e(k_1) \rightarrow \chi(p_2)e(k_2)$ is given by

$$\begin{aligned} \mathcal{M} = & \frac{G_F}{\sqrt{2}} \bar{u}_\chi(p_2) P_L u_\nu(p_1) \bar{u}_e(k_2) (\epsilon^S + \tilde{\epsilon}^S \gamma_5) u_e(k_1) \\ & + \frac{G_F}{\sqrt{2}} \bar{u}_\chi(p_2) i\gamma_5 P_L u_\nu(p_1) \bar{u}_e(k_2) i\gamma_5 (\epsilon^P + \tilde{\epsilon}^P \gamma_5) u_e(k_1) \\ & + \frac{G_F}{\sqrt{2}} \bar{u}_\chi(p_2) \gamma_\mu P_L u_\nu(p_1) \bar{u}_e(k_2) \gamma^\mu (\epsilon^V + \tilde{\epsilon}^V \gamma_5) u_e(k_1) \\ & + \frac{G_F}{\sqrt{2}} \bar{u}_\chi(p_2) \gamma_\mu \gamma_5 P_L u_\nu(p_1) \bar{u}_e(k_2) \gamma^\mu \gamma_5 (\epsilon^A + \tilde{\epsilon}^A \gamma_5) u_e(k_1) \end{aligned}$$

$$\begin{aligned}
& + \frac{G_F}{\sqrt{2}} \bar{u}_\chi(p_2) \sigma_{\mu\nu} P_L u_\nu(p_1) \bar{u}_e(k_2) \sigma^{\mu\nu} (\epsilon^T + \tilde{\epsilon}^T \gamma_5) u_e(k_1) \\
& + \frac{i G_F v_H e Q_e}{t^2} \bar{u}_\chi(p_2) \sigma_{\mu\nu} (\epsilon^M + \epsilon^E \gamma_5) P_L u_\nu(p_1) \bar{u}_e(k_2) \gamma_\mu t_\nu u_e(k_1) ,
\end{aligned} \tag{A1}$$

where the projector $P_L = (1 - \gamma_5)/2$ is inserted to force the incoming neutrinos to be left-handed and $t = p_1 - p_2$. The amplitude for $\bar{\nu}(p_1) e(k_1) \rightarrow \bar{\chi}(p_2) e(k_2)$ is given by

$$\begin{aligned}
\mathcal{M} = & \frac{G_F}{\sqrt{2}} \bar{\nu}_\nu(p_1) P_R v_\chi(p_2) \bar{u}_e(k_2) (\epsilon^{S*} - \tilde{\epsilon}^{S*} \gamma_5) u_e(k_1) \\
& + \frac{G_F}{\sqrt{2}} \bar{\nu}_\nu(p_1) P_R i \gamma_5 v_\chi(p_2) \bar{u}_e(k_2) i \gamma_5 (\epsilon^{P*} - \tilde{\epsilon}^{P*} \gamma_5) u_e(k_1) \\
& + \frac{G_F}{\sqrt{2}} \bar{\nu}_\nu(p_1) P_R \gamma_\mu v_\chi(p_2) \bar{u}_e(k_2) \gamma^\mu (\epsilon^{V*} + \tilde{\epsilon}^{V*} \gamma_5) u_e(k_1) \\
& + \frac{G_F}{\sqrt{2}} \bar{\nu}_\nu(p_1) P_R \gamma_\mu \gamma_5 v_\chi(p_2) \bar{u}_e(k_2) \gamma^\mu \gamma_5 (\epsilon^{A*} + \tilde{\epsilon}^{A*} \gamma_5) u_e(k_1) \\
& + \frac{G_F}{\sqrt{2}} \bar{\nu}_\nu(p_1) P_R \sigma_{\mu\nu} v_\chi(p_2) \bar{u}_e(k_2) \sigma^{\mu\nu} (\epsilon^{T*} - \tilde{\epsilon}^{T*} \gamma_5) u_e(k_1) \\
& + \frac{i G_F v_H e Q_e}{t^2} \bar{\nu}_\nu(p_1) P_R \sigma_{\mu\nu} (\epsilon^{M*} - \epsilon^{E*} \gamma_5) v_\chi(p_2) \bar{u}_e(k_2) \gamma_\mu t_\nu u_e(k_1) ,
\end{aligned} \tag{A2}$$

where the projector $P_R = (1 + \gamma_5)/2$ is inserted to force the incoming anti-neutrinos to be right-handed. The differential cross section of neutrino-electron scattering $\nu(\bar{\nu}) + e \rightarrow \chi(\bar{\chi}) + e$ is

$$\frac{d\sigma(\nu e)}{dE_R} = \frac{1}{32\pi m_e E_\nu^2} \overline{|\mathcal{M}|^2} , \tag{A3}$$

where $\overline{|\mathcal{M}|^2}$ is the spin-averaged amplitude square. The scattering angle is

$$\cos \theta = \frac{E_R(E_\nu + m_e) + m_\chi^2/2}{E_\nu \sqrt{E_R^2 + 2m_e E_R}} . \tag{A4}$$

By requiring $\cos \theta \leq 1$, we can get the bounds on E_R as

$$E_R^{\min(\max)} = \frac{2m_e E_\nu^2 - m_\chi^2(m_e + E_\nu) \mp E_\nu \sqrt{(2m_e E_\nu - m_\chi^2)^2 - 4m_e^2 m_\chi^2}}{2m_e(m_e + 2E_\nu)} , \tag{A5}$$

and the minimal energy to generate the elastic scattering is

$$E_\nu^{\min} = m_\chi + \frac{m_\chi^2}{2m_e} . \tag{A6}$$

-
- [1] P. A. Zyla et al. (Particle Data Group), [PTEP **2020**, 083C01 \(2020\)](#).
[2] V. Brdar, W. Rodejohann, and X.-J. Xu, [JHEP **12**, 024 \(2018\)](#), [arXiv:1810.03626 \[hep-ph\]](#).
[3] W.-F. Chang and J. N. Ng, [Phys. Rev. D **101**, 035028 \(2020\)](#), [arXiv:1903.12545 \[hep-ph\]](#).

- [4] J. A. Dror, G. Elor, and R. McGehee, *Phys. Rev. Lett.* **124**, 18 (2020), [arXiv:1905.12635 \[hep-ph\]](#).
- [5] J. A. Dror, G. Elor, and R. McGehee, *JHEP* **02**, 134 (2020), [arXiv:1908.10861 \[hep-ph\]](#).
- [6] W.-F. Chang and J. Liao, *Phys. Rev. D* **102**, 075004 (2020), [arXiv:2002.10275 \[hep-ph\]](#).
- [7] T. Li, X.-D. Ma, and M. A. Schmidt, *JHEP* **07**, 152 (2020), [arXiv:2005.01543 \[hep-ph\]](#).
- [8] N. Hurtado, H. Mir, I. M. Shoemaker, E. Welch, and J. Wyenberg, *Phys. Rev. D* **102**, 015006 (2020), [arXiv:2005.13384 \[hep-ph\]](#).
- [9] T. Li and J. Liao, *JHEP* **02**, 099 (2021), [arXiv:2008.00743 \[hep-ph\]](#).
- [10] S.-F. Ge, P. Pasquini, and J. Sheng, *Phys. Lett. B* **810**, 135787 (2020), [arXiv:2006.16069 \[hep-ph\]](#).
- [11] I. M. Shoemaker, Y.-D. Tsai, and J. Wyenberg, (2020), [arXiv:2007.05513 \[hep-ph\]](#).
- [12] S. Shakeri, F. Hajkarim, and S.-S. Xue, (2020), [arXiv:2008.05029 \[hep-ph\]](#).
- [13] J. A. Dror, G. Elor, R. McGehee, and T.-T. Yu, (2020), [arXiv:2011.01940 \[hep-ph\]](#).
- [14] V. Brdar, A. Greljo, J. Kopp, and T. Opferkuch, *JCAP* **01**, 039 (2021), [arXiv:2007.15563 \[hep-ph\]](#).
- [15] D. Aristizabal Sierra, R. Branada, O. G. Miranda, and G. Sanchez Garcia, *JHEP* **12**, 178 (2020), [arXiv:2008.05080 \[hep-ph\]](#).
- [16] E. Aprile *et al.* (XENON), *Phys. Rev. D* **102**, 072004 (2020), [arXiv:2006.09721 \[hep-ex\]](#).
- [17] N. Viaux, M. Catelan, P. B. Stetson, G. Raffelt, J. Redondo, A. A. R. Valcarce, and A. Weiss, *Phys. Rev. Lett.* **111**, 231301 (2013), [arXiv:1311.1669 \[astro-ph.SR\]](#).
- [18] S. A. Díaz, K.-P. Schröder, K. Zuber, D. Jack, and E. E. B. Barrios, (2019), [arXiv:1910.10568 \[astro-ph.SR\]](#).
- [19] L. Di Luzio, M. Fedele, M. Giannotti, F. Mescia, and E. Nardi, *Phys. Rev. Lett.* **125**, 131804 (2020), [arXiv:2006.12487 \[hep-ph\]](#).
- [20] C. Gao, J. Liu, L.-T. Wang, X.-P. Wang, W. Xue, and Y.-M. Zhong, *Phys. Rev. Lett.* **125**, 131806 (2020), [arXiv:2006.14598 \[hep-ph\]](#).
- [21] J. B. Dent, B. Dutta, J. L. Newstead, and A. Thompson, *Phys. Rev. Lett.* **125**, 131805 (2020), [arXiv:2006.15118 \[hep-ph\]](#).
- [22] M. Agostini *et al.* (Borexino), *Phys. Rev. D* **100**, 082004 (2019), [arXiv:1707.09279 \[hep-ex\]](#).
- [23] P. Vilain *et al.* (CHARM-II), *Phys. Lett. B* **302**, 351 (1993).
- [24] P. Vilain *et al.* (CHARM-II), *Phys. Lett. B* **335**, 246 (1994).
- [25] M. Deniz *et al.* (TEXONO), *Phys. Rev. D* **81**, 072001 (2010), [arXiv:0911.1597 \[hep-ex\]](#).
- [26] A. N. Khan, W. Rodejohann, and X.-J. Xu, *Phys. Rev. D* **101**, 055047 (2020), [arXiv:1906.12102 \[hep-ph\]](#).
- [27] A. G. Beda, E. V. Demidova, A. S. Starostin, V. B. Brudanin, V. G. Egorov, D. V. Medvedev, M. V. Shirchenko, and T. Vylov, *Phys. Part. Nucl. Lett.* **7**, 406 (2010), [arXiv:0906.1926 \[hep-ex\]](#).
- [28] L. B. Auerbach *et al.* (LSND), *Phys. Rev. D* **63**, 112001 (2001), [arXiv:hep-ex/0101039](#).
- [29] J. Liao, D. Marfatia, and K. Whisnant, *Phys. Lett. B* **771**, 247 (2017), [arXiv:1704.04711 \[hep-ph\]](#).
- [30] G. Bellini *et al.* (Borexino), *Phys. Lett. B* **707**, 22 (2012), [arXiv:1104.2150 \[hep-ex\]](#).
- [31] G. Bellini *et al.*, *Phys. Rev. Lett.* **107**, 141302 (2011), [arXiv:1104.1816 \[hep-ex\]](#).
- [32] G. Bellini *et al.* (Borexino), *Phys. Rev. Lett.* **108**, 051302 (2012), [arXiv:1110.3230 \[hep-ex\]](#).

- [33] G. Bellini et al. (Borexino), [Phys. Rev. D **89**, 112007 \(2014\)](#), [arXiv:1308.0443 \[hep-ex\]](#).
- [34] G. Bellini et al. (BOREXINO), [Nature **512**, 383 \(2014\)](#).
- [35] M. Agostini et al. (Borexino), [Phys. Rev. D **101**, 062001 \(2020\)](#), [arXiv:1709.00756 \[hep-ex\]](#).
- [36] N. Vinyoles, A. M. Serenelli, F. L. Villante, S. Basu, J. Bergström, M. Gonzalez-Garcia, M. Maltoni, C. Peña Garay, and N. Song, [Astrophys. J. **835**, 202 \(2017\)](#), [arXiv:1611.09867 \[astro-ph.SR\]](#).
- [37] K. Kannike, M. Raidal, H. Veermäe, A. Strumia, and D. Teresi, (2020), [arXiv:2006.10735 \[hep-ph\]](#).
- [38] R. Essig, J. Mardon, and T. Volansky, [Phys. Rev. D **85**, 076007 \(2012\)](#), [arXiv:1108.5383 \[hep-ph\]](#).
- [39] R. Essig, M. Fernandez-Serra, J. Mardon, A. Soto, T. Volansky, and T.-T. Yu, [JHEP **05**, 046 \(2016\)](#), [arXiv:1509.01598 \[hep-ph\]](#).
- [40] P. Ade et al. (Planck), [Astron. Astrophys. **594**, A13 \(2016\)](#), [arXiv:1502.01589 \[astro-ph.CO\]](#).